AD-A174 295 COMPUTATIONS SUPERSONIC FLOW OVER A MISSILE AFTERBODY CONTAINING AN EXHAUST JET(U) ARMY BALLISTIC RESEARCH LAB ABERDEEN PROVING GROUND MD J SAHU SEP 86 1/1

UNCLASSIFIED BRL-MR-3548 F/G 20/4 NL

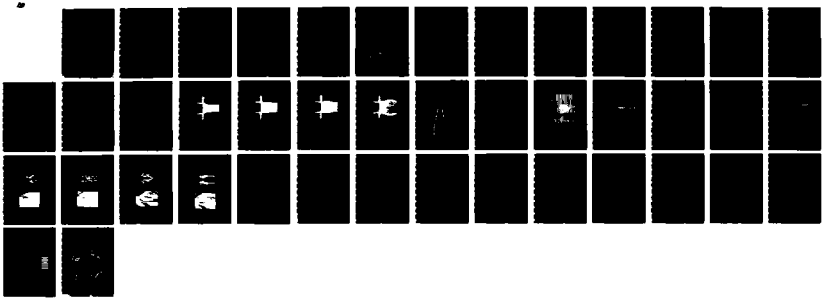

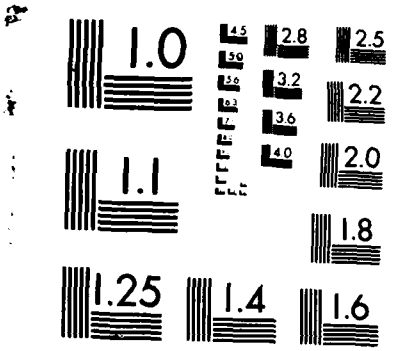

(12)

AD

US ARMY MATERIEL COMMAND

MEMORANDUM REPORT BRL-MR-3548

AD-A174 295

COMPUTATIONS OF SUPERSONIC FLOW OVER A MISSILE AFTERBODY CONTAINING AN EXHAUST JET

Jubaraj Sahu

September 1986

US ARMY BALLISTIC RESEARCH LABORATORY
ABERDEEN PROVING GROUND, MARYLAND

Destroy this report when it is no longer needed.
Do not return it to the originator.

Additional copies of this report may be obtained from the National Technical Information Service, U. S. Department of Commerce, Springfield, Virginia 22161.

The findings in this report are not to be construed as an official Department of the Army position, unless so designated by other authorized documents.

The use of trade names or manufacturers' names in this report does not constitute indorsement of any commercial product.

UNCLASSIFIED

SECURITY CLASSIFICATION OF THIS PAGE

AD-A174 345

REPORT DOCUMENTATION PAGE

Form Approved
OMB No 0704-0188
Exp Date Jun 30 1986

1a REPORT SECURITY CLASSIFICATION UNCLASSIFIED	1b. RESTRICTIVE MARKINGS
2a. SECURITY CLASSIFICATION AUTHORITY	3 DISTRIBUTION / AVAILABILITY OF REPORT Approved for public release, distribution unlimited.
2b. DECLASSIFICATION / DOWNGRADING SCHEDULE	
4 PERFORMING ORGANIZATION REPORT NUMBER(S) Memorandum Report BRL-MR-3548	5. MONITORING ORGANIZATION REPORT NUMBER(S)
6a. NAME OF PERFORMING ORGANIZATION U.S. Army Ballistic Research Laboratory 6b. OFFICE SYMBOL (If applicable) SLCBR-LF	7a. NAME OF MONITORING ORGANIZATION
6c. ADDRESS (City, State, and ZIP Code) Aberdeen Proving Ground, Maryland 21005-5066	7b. ADDRESS (City, State, and ZIP Code)
8a. NAME OF FUNDING / SPONSORING ORGANIZATION 8b. OFFICE SYMBOL (If applicable)	9. PROCUREMENT INSTRUMENT IDENTIFICATION NUMBER
8c. ADDRESS (City, State, and ZIP Code)	10. SOURCE OF FUNDING NUMBERS PROGRAM ELEMENT NO. 62618A; PROJECT NO. 1L162618AH80; TASK NO. 00; WORK UNIT ACCESSION NO 001 AJ

11. TITLE (Include Security Classification)

COMPUTATIONS OF SUPERSONIC FLOW OVER A MISSILE AFTERBODY CONTAINING AN EXHAUST JET

12. PERSONAL AUTHOR(S)
SAHU, JUBARAJ

13a. TYPE OF REPORT	13b. TIME COVERED	14. DATE OF REPORT (Year, Month, Day)	15. PAGE COUNT
Memorandum Report	FROM _____ TO _____	September 1986	43

16. SUPPLEMENTARY NOTATION

17. COSATI CODES		
FIELD	GROUP	SUB-GROUP
01	01	
16	04	

18. SUBJECT TERMS (Continue on reverse if necessary and identify by block number)
Navier-Stokes Computations; Base Flow; Propulsive Jet; Supersonic Speed; Implicit Algorithm; Missile Afterbody

19. ABSTRACT (Continue on reverse if necessary and identify by block number)

A thin-layer Navier-Stokes code, developed for projectile aerodynamics, has been used to compute the supersonic flow over a missile afterbody containing a centered exhaust jet. The thin-layer, compressible, Navier-Stokes equations are solved using a time dependent, implicit numerical algorithm. A unique flow field segmentation procedure is used which preserves the sharp base corner and facilitates the adaption of the grid to the free shear layer in the base region. Solutions have been obtained for an axisymmetric, boattailed afterbody where the free stream Mach number is 2.0 and the jet exit Mach number is 2.5. Computations were made at various jet static pressure to free stream static pressure ratios from 1 through 9. Qualitative features of the base region flow field seen experimentally are very well observed in the computed results. Quantitative comparisons of base pressure with experiment indicate good agreement at high pressure ratios and some disagreement at low pressure ratios.

20 DISTRIBUTION / AVAILABILITY OF ABSTRACT	21 ABSTRACT SECURITY CLASSIFICATION
☒ UNCLASSIFIED/UNLIMITED ☐ SAME AS RPT ☐ DTIC USERS	UNCLASSIFIED
22a NAME OF RESPONSIBLE INDIVIDUAL Jubaraj Sahu	22b TELEPHONE (Include Area Code) (301) 278-3707
	22c OFFICE SYMBOL SLCBR-LF-R

DD FORM 1473, 84 MAR 83 APR edition may be used until exhausted
All other editions are obsolete

SECURITY CLASSIFICATION OF THIS PAGE

UNCLASSIFIED

18. Subject Terms (Continued)

Plume Shape

Compressible

TABLE OF CONTENTS

LIST OF FIGURES

I. INTRODUCTION

The flow field in the base region of a jet-propelled tactical missile or a rocket-assisted artillery projectile is complex. The propulsive jet is underexpanded and can strongly affect the base pressure distribution and the afterbody flow field. For large jet to free stream pressure ratios, the interaction of the exhaust jet with the external flow can be large enough to induce extensive afterbody flow separation. This can, of course, seriously affect the control effectiveness of any control surface located in that region. For over a decade, experimental efforts and the component approach of Korst[1] has provided valuable insight into this flow problem. The flow field under consideration is complicated due to strong viscous/inviscid interaction and regions of flow separation. The component approach has its serious limitations for three-dimensional configurations and similar procedures are extremely difficult to apply at transonic speeds.[2]

Recent advances in numerical algorithms and the advent of supercomputers have made numerical modeling of the Navier-Stokes equations a reality. As computational speed has sharply increased, the computing costs have sharply dropped. This trend in technology makes the direct solution of Navier-Stokes equations even more attractive. The Navier-Stokes computational technique models the strong interactions involved between the flow regimes in a fully coupled manner and does not contain the empiricism found in the component approach. Some empiricism does enter into the Navier-Stokes solutions through turbulence modeling which is an area of further computational and experimental research.

Recently, Sahu, et al,[3] computed the base region flow field for a projectile at transonic speeds using the thin layer Navier-Stokes equations. A unique flow field segmentation procedure was used for complete numerical simulation of a projectile including the base region. This technique was also used to calculate the effect of a centered jet on the base region flow field at a high transonic speed.[4] Other Navier-Stokes solutions have been obtained for flow over afterbodies with exhaust jet.[5-8] The work of Deiwert[5] and Fox[6] are based on the thin-layer approximation of the Navier-Stokes equations whereas Wagner[7] and Thomas[8] solved the full Navier-Stokes equations. The two-layer, algebraic, Baldwin-Lomax[9] turbulence model was used in References 3-7. Thomas, et al[8] used the two-equation k-ε and k-w turbulence models and some differences in the computed results were observed.

This report describes the computational investigation of the effect of exhaust jet on the base pressure and the base region flow field at supersonic speed using the same numerical procedure of References 3 and 4. A unique flow field segmentation procedure, equivalent to using multiple adjoining grids, is used which preserves the sharp base corner. Additionally, the grids in the base region were adapted to the free shear layer as the solutions developed. Solutions have been obtained for supersonic flow over an axisymmetric boattail afterbody where the free stream Mach number is 2.0 and the jet exit Mach number is 2.5. Ratios of jet static pressure to free stream static pressure are considered in the range of 1 to 9 for a conical nozzle exit half angle of 20°. Comparison of the numerical results have been made with available experimental data.

II. COMPUTATIONAL TECHNIQUE

The Azimuthal Invariant (or Generalized Axisymmetric) thin-layer Navier-Stokes equations for general spatial coordinates ξ, η, ζ can be written as[10]

$$\partial_\tau \hat{q} + \partial_\xi \hat{E} + \partial_\zeta \hat{G} + \hat{H} = Re^{-1} \partial_\zeta \hat{S} \tag{1}$$

where $\xi = \xi(x,y,z,t)$ is the longitudinal coordinate

$\eta = \eta(y,z,t)$ is the circumferential coordinate

$\zeta = \zeta(x,y,z,t)$ is the near normal coordinate

$\tau = t$ is the time

and

$$\hat{q} = J^{-1} \begin{bmatrix} \rho \\ \rho u \\ \rho v \\ \rho w \\ e \end{bmatrix}, \quad \hat{E} = J^{-1} \begin{bmatrix} \rho U \\ \rho uU + \xi_x p \\ \rho vU + \xi_y p \\ \rho wU + \xi_z p \\ (e+p)U - \xi_t p \end{bmatrix},$$

$$\hat{G} = J^{-1} \begin{bmatrix} \rho W \\ \rho uW + \zeta_x p \\ \rho vW + \zeta_y p \\ \rho wW + \zeta_z p \\ (e+p)W - \zeta_t p \end{bmatrix},$$

$$\hat{H} = J^{-1} \begin{bmatrix} 0 \\ 0 \\ \rho V[R_\xi(U-\xi_t) + R_\zeta(W-\zeta_t)] \\ -\rho VR(V-\eta_t) - p/R \\ 0 \end{bmatrix}$$

$$\hat{S} = \begin{bmatrix} 0 \\ \mu(\zeta_x^2+\zeta_y^2+\zeta_z^2)u_\zeta + (\mu/3)(\zeta_x u_\zeta+\zeta_y v_\zeta+\zeta_z w_\zeta)\zeta_x \\ \mu(\zeta_x^2+\zeta_y^2+\zeta_z^2)v_\zeta + (\mu/3)(\zeta_x u_\zeta+\zeta_y v_\zeta+\zeta_z w_\zeta)\zeta_y \\ \mu(\zeta_x^2+\zeta_y^2+\zeta_z^2)w_\zeta + (\mu/3)(\zeta_x u_\zeta+\zeta_y v_\zeta+\zeta_z w_\zeta)\zeta_z \\ \{(\zeta_x^2+\zeta_y^2+\zeta_z^2)[(\mu/2)(u^2+v^2+w^2)_\zeta \\ \quad + \kappa Pr^{-1}(\gamma-1)^{-1}(a^2)_\zeta] + (\mu/3) \\ \quad (\zeta_x u+\zeta_y v+\zeta_z w)(\zeta_x u_\zeta+\zeta_y v_\zeta+\zeta_z w_\zeta)\} \end{bmatrix}$$

The velocities

$$U = \xi_t + \xi_x u + \xi_y v + \xi_z w$$

$$V = \eta_t + \eta_x u + \eta_y v + \eta_z w$$

$$W = \zeta_t + \zeta_x u + \zeta_y v + \zeta_z w$$

represent the contravariant velocity components.

The Cartesian velocity component (u, v, w) are nondimensionalized with respect to a_∞ (free stream speed of sound). The density (ρ) is referenced to ρ_∞ and total energy (e) to $\rho_\infty a_\infty^2$. The local pressure is determined using the equation of state,

$$p = (\gamma - 1)[e - 0.5\rho(u^2 + v^2 + w^2)] \qquad (3)$$

where γ is the ratio of specific heats.

In Equation (1), axisymmetric flow assumptions have been made which result in the source term, $\hat{H}$. The details of how this is obtained can be found in Reference 10 and are not discussed here. Equation (1) contains only two spatial derivatives. However, it retains all three momentum equations and allows a degree of generality over the standard axisymmetric equations. In particular, the circumferential velocity is not assumed to be zero thus allowing computations for spinning projectiles to be accomplished.

The numerical algorithm used is the Beam-Warming fully implicit, approximately factored finite difference scheme. The algorithm can be first or second order accurate in time and second or fourth order accurate in space. Since the interest is only in the steady-state solution, Equation (1) is solved in a time asymptotic fashion and first order accurate time differencing is used. The spatial accuracy is fourth order. Details of the algorithm are included in References 11-13.

For the computation of turbulent flows a turbulence model must be supplied. In the present calculations a two-layer algebraic eddy viscosity model by Baldwin and Lomax[9] is used. In their two layer model the inner region follows the Prandtl-Van Driest formulation. Their outer formulation can be used in wakes as well as in attached and separated boundary layers. In both the inner and outer formulations the distribution of vorticity is used to determine length scales thereby avoiding the necessity of finding the outer edge of the boundary layer (or wake). The magnitude of the local vorticity for the axisymmetric formulation is given by

$$|\omega| = \sqrt{(\frac{\partial u}{\partial x})^2 + (\frac{\partial v}{\partial z} - \frac{\partial w}{\partial y})^2 + (\frac{\partial w}{\partial x} - \frac{\partial u}{\partial z})^2} \tag{4}$$

In determining the outer length scale a function[9]

$$F(y) = y|\omega| \, [1 - \exp(-y^+/A^+)] \tag{5}$$

is used where y^+ and A^+ are the conventional boundary layer terms. For the base flow (or wake flow) the exponential term of Equation (5) is set equal to zero. In other words, the Van Driest damping term is not applicable and is thus neglected. The outer formulation also requires the computation of the Klebanoff intermittency function and a velocity scale U_{dif} given by

$$U_{dif} = (u^2 + v^2 + w^2)^{1/2}_{max} - (u^2 + v^2 + w^2)^{1/2}_{min} \tag{6}$$

Both of the terms on the right-hand side of Equation (6) are evaluated via the velocity profiles. For wall-bounded flows, the minimum term in U_{dif} is usually zero. For wakes, the Klebanoff intermittency factor is determined by measuring the distance from the centerline of symmetry. The algebraic eddy viscosity model may not be strictly valid for all of the wake flow situations. More realistic or complex turbulence models much be considered a subject left for future study.

III. METHOD OF SOLUTION

1. BASE REGION FLOW WITH JET-OFF

The procedure used to compute the base flow without jet for a projectile configuration has been described in Reference 3; however, limited details will

be repeated here for clarity. The code can compute the full flow field (including the base region) of a projectile. However, for supersonic flow the forebody solution can be obtained efficiently using a space-marching Parabolized Navier-Stokes (PNS) code. This technique is used to provide upstream boundary condition (line EF, Figure 1) for the computation of the afterbody flow field containing the base region. The afterbody solution is obtained using the unsteady or time-marching Navier-Stokes equations. Figure 1 shows a schematic illustration of the flow field segmentation used in this study for computational purposes. It shows the transformation of the physical domain into the computational domain and the details of the flow field segmentation procedure in both domains. This flow field segmentation procedure is equivalent to using multiple adjoining grids. An important advantage of this procedure lies in the preservation of the sharp corner at the base and allows easy blending of the computational meshes between the regions ABCD and AEFG. No approximation of the actual sharp corner at the base is made and is inherent in the current procedure.

In Figure 1, the cross hatched region represents the model. The line BC is the base and the region ABCD is the base region or the wake. The line AB is a computational cut through the physical wake region which acts as a repetitive boundary in the computational domain. Implicit integration is carried out in both ξ and ζ directions. Note the presence of the lines BC (base) and EF in the computational domain. They both act as boundaries in the computational domain and special care must be taken in inverting the block tridiagonal matrix in the ξ direction. The details of this procedure can be found in Reference 3 and are not included here.

The no slip boundary condition for viscous flow is enforced by setting

$$U = V = W = 0 \tag{7}$$

on the body surface including the base. Along the computational cut (AB), the flow variables above and below the cut are simply averaged to determine the boundary conditions on the cut. On the centerline of the wake region, a symmetry condition is imposed and free stream conditions are used on the outer boundary.

2. BASE REGION FLOW WITH JET-ON

The method of solution for the case with a centered propulsive jet remains essentially the same as described in Section III A. The boundary conditions on the body surface, at the cut and the downstream boundary also remain the same as previously described. Along the base boundary, the same conditions described earlier are used. For the nozzle exit, boundary conditions are used based on the nozzle exit Mach number, stagnation temperature and pressure. The velocity components are linearly interpolated from the center line of symmetry to the nozzle height at the exit, i.e., conical flow at the jet exit has been assumed.

IV. MODEL AND COMPUTATIONAL GRID

The model geometry used in this study comprised of a 2 caliber 14° half-angle conical nose, 6 caliber cylindrical mid-section and a 1 caliber 8° boattail. The nozzle exit diameter is 0.6 calibers. Detailed experimental measurements for this shape and the same flow conditions described earlier have been made by Agrell, et al.[14]

When computations over the entire model are made, only a limited number of grid points can be used in the base region. One way to eliminate this restriction is to use known data given by experiment or otherwise at a station upstream of the base and then compute the flow field in the isolated base region only. This, of course, allows a large number of grid points to be used in the base region and can be used to determine grid dependancy on the computed solution in the base region. This is ideally suited for the numerical computations of base region flow field at supersonic velocities. Solutions can be obtained for the forebody with the space-marching PNS code. In the present study, the PNS code was used to generate a solution at a station 1.5 calibers upstream of the base; and this solution was then used as an upstream boundary condition for the computation of the base region flow field by the unsteady base flow code.

Figures 2-5 show the expanded view of the computational grids in the base region. These grids are shown for both upper and lower halves for clarity; however, computations are made only for the upper half plane for axisymmetric flow. Figure 2 shows the grid for the jet-off case whereas the grids shown in Figures 3-5 are for the jet-on cases of P_j/P_∞ = 1, 3 and 9, respectively. Additionally, these grids were adapted to the free shear layer as the solutions developed. Logic has been implemented to adjust the grid cut AB (Figure 1) to the viscous shear layer which begins to neck-down shortly behind the base. The height of the cut is weighted between a moment of shear and the standard nonadaptive grids. Specifically, the cut height $\bar{z}$, at each j location is determined by the relation

$$\bar{z}_j = \frac{\Sigma(\delta_z u_{j\ell})^2 \, z_{j\ell} + \varepsilon D/2}{\Sigma \, (\delta_z u_{j\ell})^2 + \varepsilon} \tag{8}$$

where the ℓ summation is carried out only for those points within an interval $0.2D \leq z_{j\ell} \leq 2D$. Here D is the base diameter, δ_z a central difference operator, and ε a positive parameter that ensures a standard grid if all $\delta_z u_{j\ell}$ are zero or if ε is very large. Additional averaging is used in the x direction (longitudinal direction). Each of these grids consisted of 200 points in the longitudinal direction with 80 points located in the base region and 50 points in the normal direction. Details of the grid patching used consistent with the flow field segmentation procedure and the strategy of clustering of grid points can be found in References 3 and 4.

V. RESULTS

All the computations were made at $M_\infty = 2.0$, $\alpha = 0$ and for a jet exit Mach number of 2.5. Solutions were obtained for the jet-off case and jet-on cases for jet-to-free-stream pressure ratios, $P_j/P_\infty = 1$, 3 and 9. Figure 6 shows a schematic illustration of the base flow for the jet-on condition and its associated nomenclature.

Figure 7 shows the velocity vectors in the base region for the jet-off case. The recirculatory flow in the near wake is clearly evident. The expected velocity defect can also be seen further downstream in this figure. The effect of the centered propulsive jet on the base region flow field is shown in Figures 8-10 for $P_j/P_\infty = 1$, 3, and 9, respectively. Figure 8a shows the velocity vectors in the near wake for a pressure ratio of 1. The flow field in the base region has changed considerably and the large recirculatory bubble seen for the jet-off condition is much reduced. This small separation bubble is a region of counter clockwise recirculating flow and can be seen near the base corner as shown in Figure 8b. Similar features can be seen for the pressure ratio, $P_j/P_\infty = 3$ as shown in Figure 9. In both Figures 8 and 9, one can observe the oblique compression shock wave at the end of the afterbody and the barrel shock inside the plume indicated by the turning of the velocity vectors. Figure 10a shows the velocity vectors for the high pressure ratio case of $P_j/P_\infty = 9$. The shape of the plume is clearly shown. An expanded view of the flow field near the end of the afterbody and the base corner is shown in Figure 10b. This figure shows an extensive region of flow separation upstream of the base corner. The small separation bubble seen downstream of the base corner for the lower pressure ratio case is virtually eliminated. The separation bubble upstream of the base corner is confined to the boundary layer on the afterbody. Additionally, the compression shock wave seen at the end of the afterbody with the lower jet pressure has now moved further upstream of the base corner with the high jet exit pressure.

The next four Figures 11-14 show the comparisons of the computed density contours and the experimental Schlieren pictures[9] for the jet-off case and jet-on cases with $P_j/P_\infty = 1$, 3, and 9, respectively. These Schilieren photographs are for the same geometry and flow conditions obtained from the experimental study of Agrell, et al.[14] Figure 11 shows the comparison for the jet-off condition. For this case, the expansions at the base corner, the free shear layer and the recompression shock downstream of the base are all clearly observed in the computed results and agree very well with the experimental observations. Comparisons for the jet-on conditions are shown in Figures 12-14 and it is clear that flow features in the base region have changed due to the presence of the jet. Figure 12 shows the results for the jet pressure ratio of 1. The flow features to be seen are the oblique shock at the end of the afterbody, the trailing shock system inside the plume and the slip line that emanates from the nozzle lip and defines the jet boundary. The trailing shock inside the plume closes about 1/2 caliber downstream of the exit plane and results in a Mach reflection. As the jet-to-free-stream pressure ratio is increased to 3.0, the trailing shocks inside the plume cross each other about 2 calibers downstream of the base (see Figure 13). Other features are similar to the pressure ratio of one case. Details of the flow features in the base

region are changed as the jet exit pressure ratio is increased to 9. The trailing shock system seen with the lower pressure ratios is not observed in either the computations or experiment (see Figure 14). For this higher jet pressure ratio, one can observe a lambda shock near the base corner which induces a separation region on the afterbody just upstream of the base corner. The agreement between the computed and the experimentally observed flow features is very good for both jet-off and jet-on conditions.

Quantitatively, one is interested in how the complex flow field in the base region affects the base pressure. Figure 15 shows the base pressure as a function of boattail angles for the jet-off condition. Although experimental measurements were made for various boattail angles, computations were restricted to only the 8° boattail case. The computed base pressure agrees well with the experimental data. The centered jet affects the base region flow field considerably and, thus, has a strong affect on the base pressure. The effect of the jet on the base pressure for various jet to free stream pressure ratios is shown in Figure 16. The trend of an increase in base pressure with jet pressure seen experimentally is clearly predicted by the numerical solutions. Good agreement is found at the high pressure ratio. Some disagreement, however, is observed at the lower pressure ratios.

VI. CONCLUDING REMARKS

A computational study was made for supersonic flow over a missile afterbody in the presence of a centered propulsive jet. The thin-layer form of the compressible Navier-Stokes equations was solved using a time-dependent, implicit numerical algorithm. Solutions were obtained for both jet-off and jet-on conditions for a free stream Mach number of 2.0 and the jet exit Mach number of 2.5. Three jet-to-free-stream ratios (1, 3, and 9) were considered. The grids in the base region were adapted to the free shear layer as the solutions developed. Qualitative features of the base region flow field such as the compression shock, plume shape, and trailing shock system seen experimentally were easily observed in the computed results. Quantitative comparisons indicate good agreement for the jet-off case. Also, the predicted effect of the jet on the base pressure has the correct trend observed experimentally. Some disagreement at lower pressure ratios exists. The accuracy of these predictions should improve as turbulence modeling used for these flows improves.

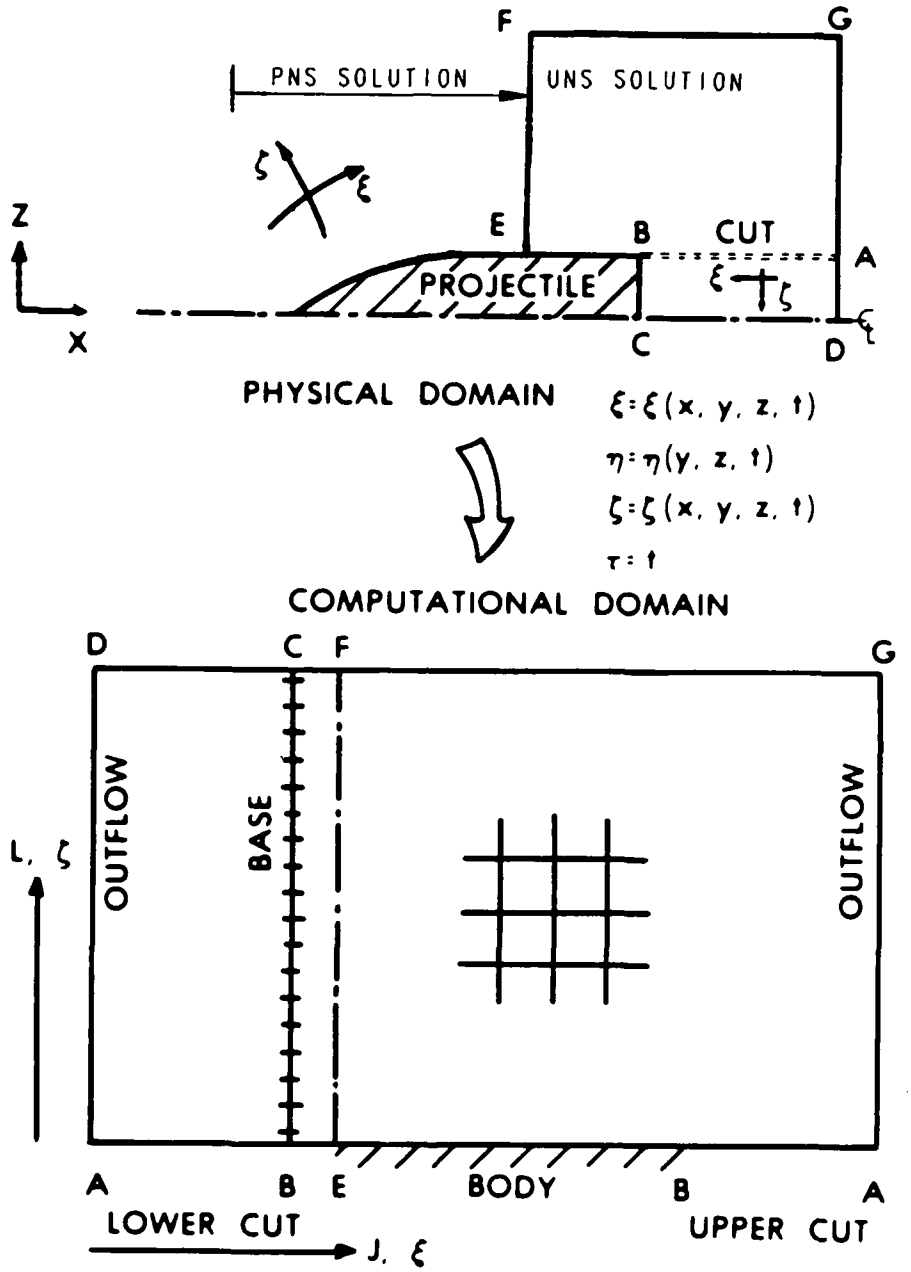

Figure 1. Schematic illustration of flow field segmentation.

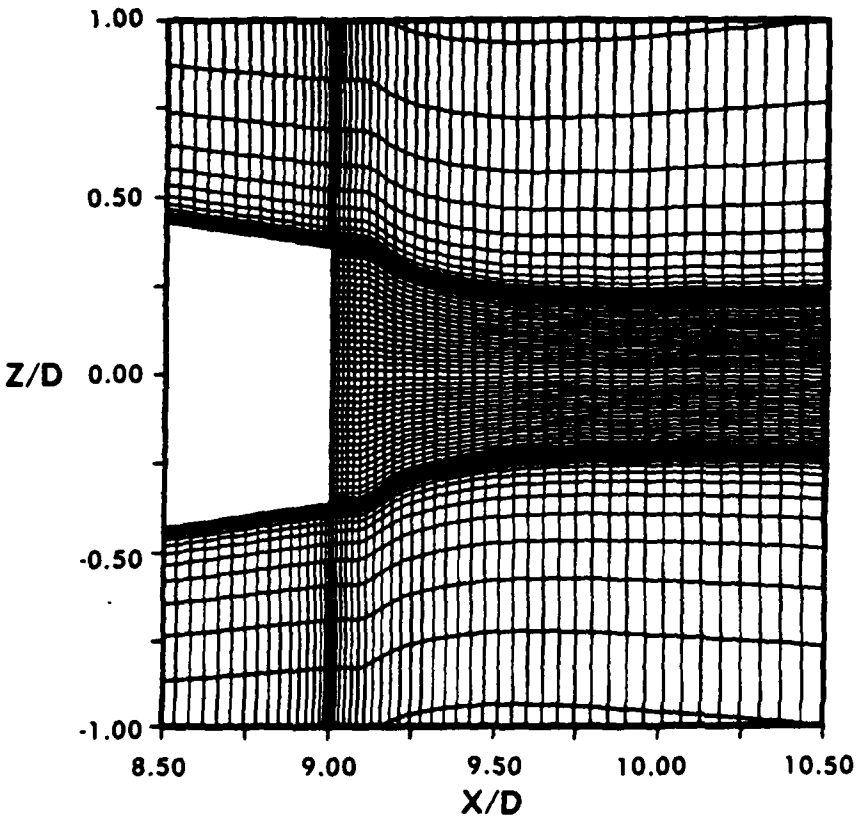

Figure 2. Computational grid in the base region, jet-off.

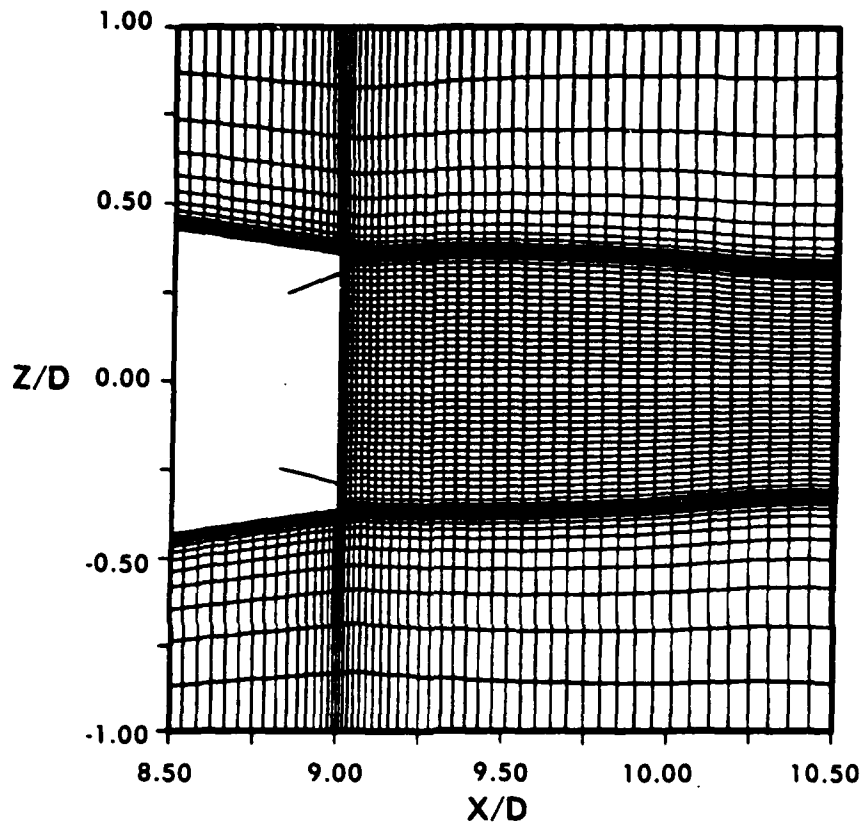

Figure 3. Computational grid in the base region, jet-on, $P_j/P_\infty = 1.0$.

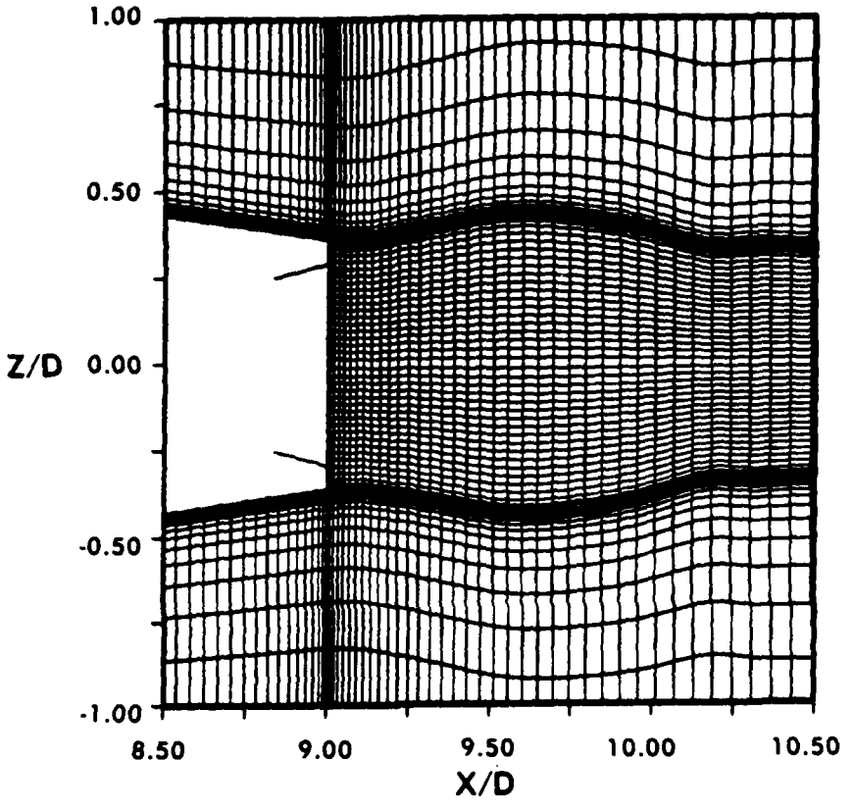

Figure 4. Computational grid in the base region, jet-on, $P_j/P_\infty = 3.0$.

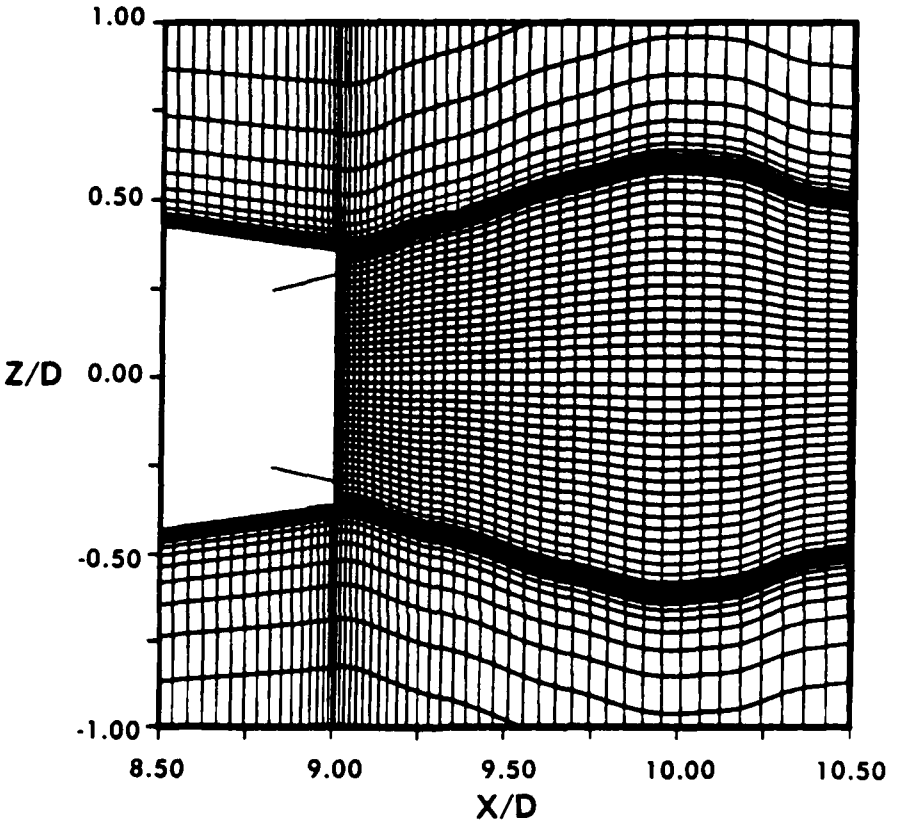

Figure 5. Computational grid in the base region, jet-on, $P_j/P_\infty = 9.0$.

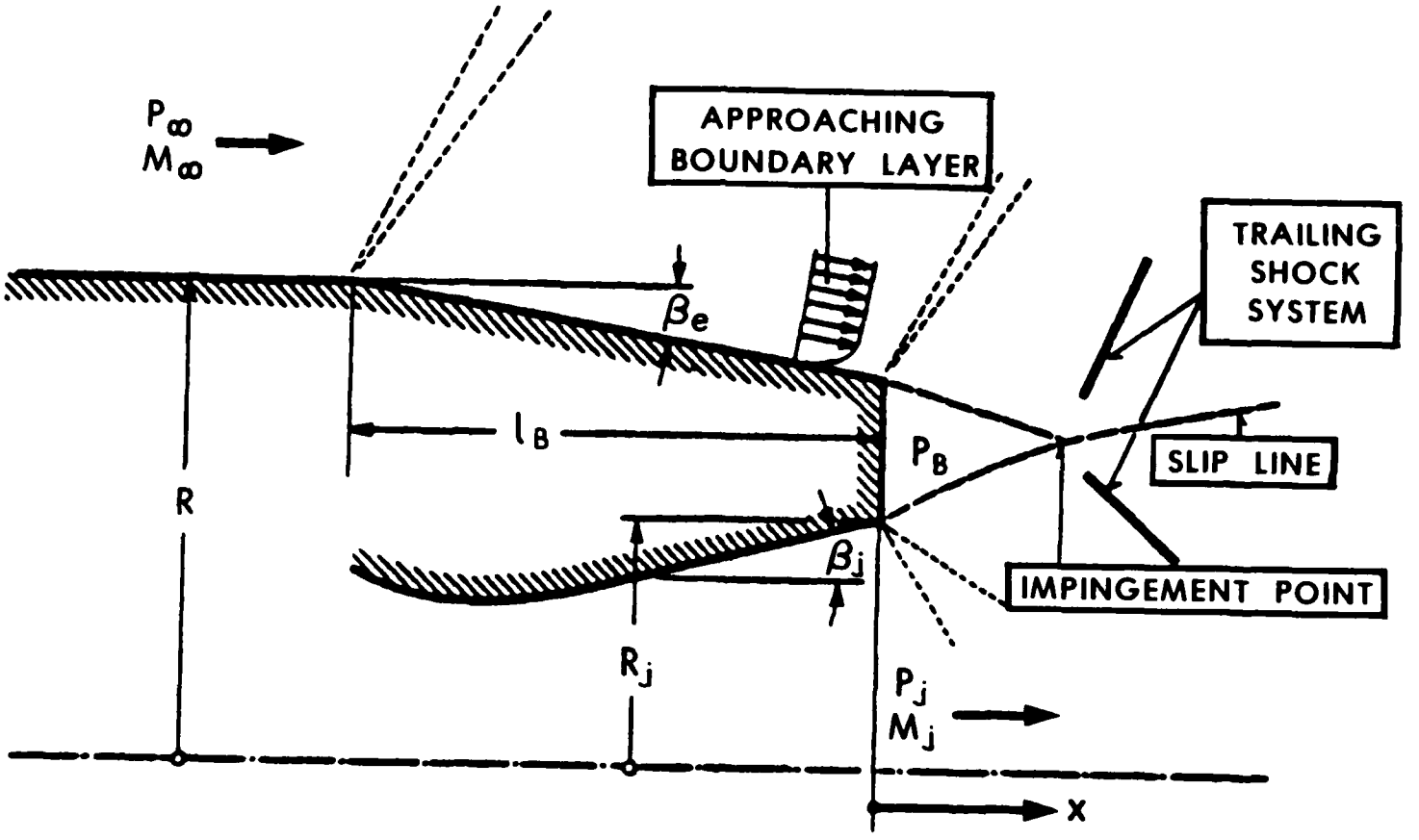

Figure 6. Schematics of the afterbody flow with jet.

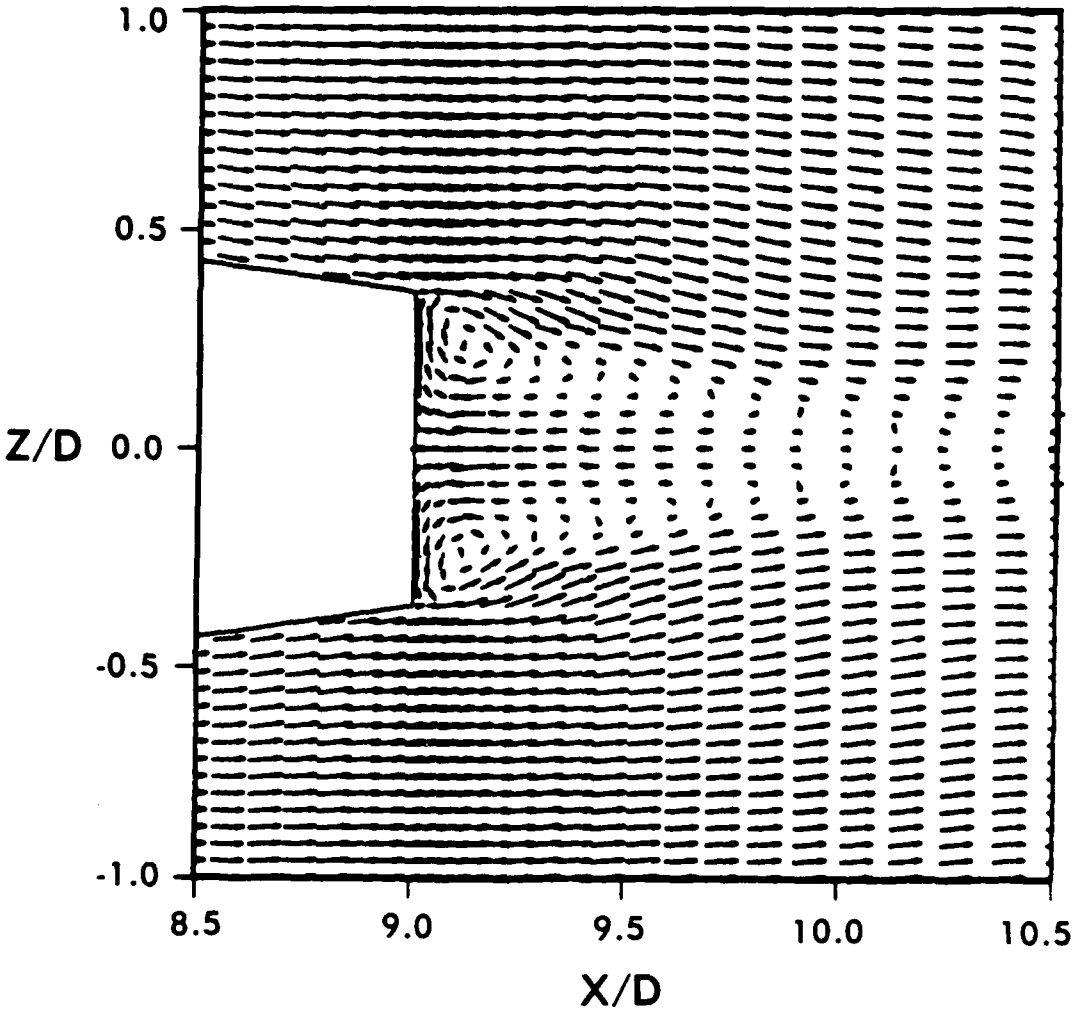

Figure 7. Velocity vectors in the base region, M_∞ = 2.0, jet-off.

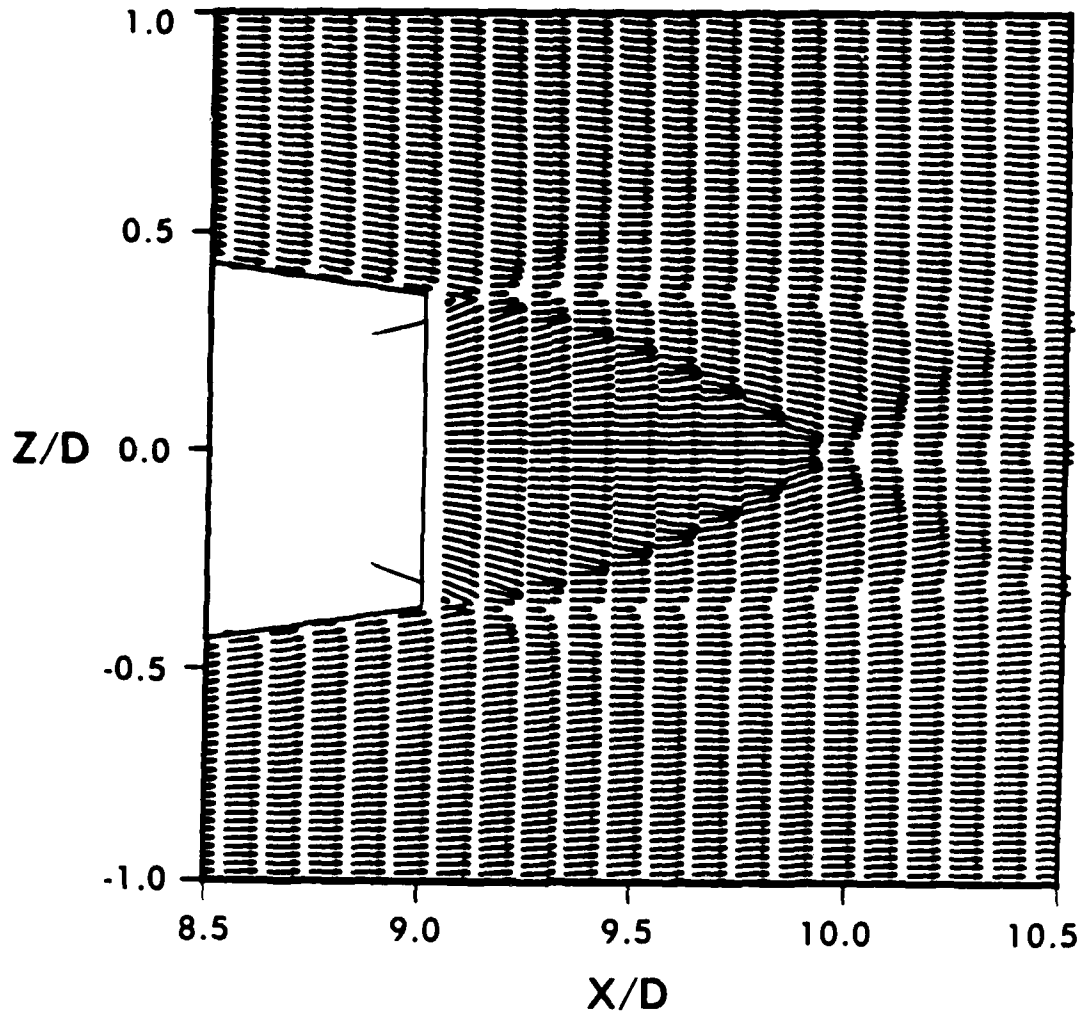

Figure 8a. Velocity vectors in the base region, M_∞ = 2.0, M_j = 2.5, P_j/P_∞ = 1.0, jet-on.

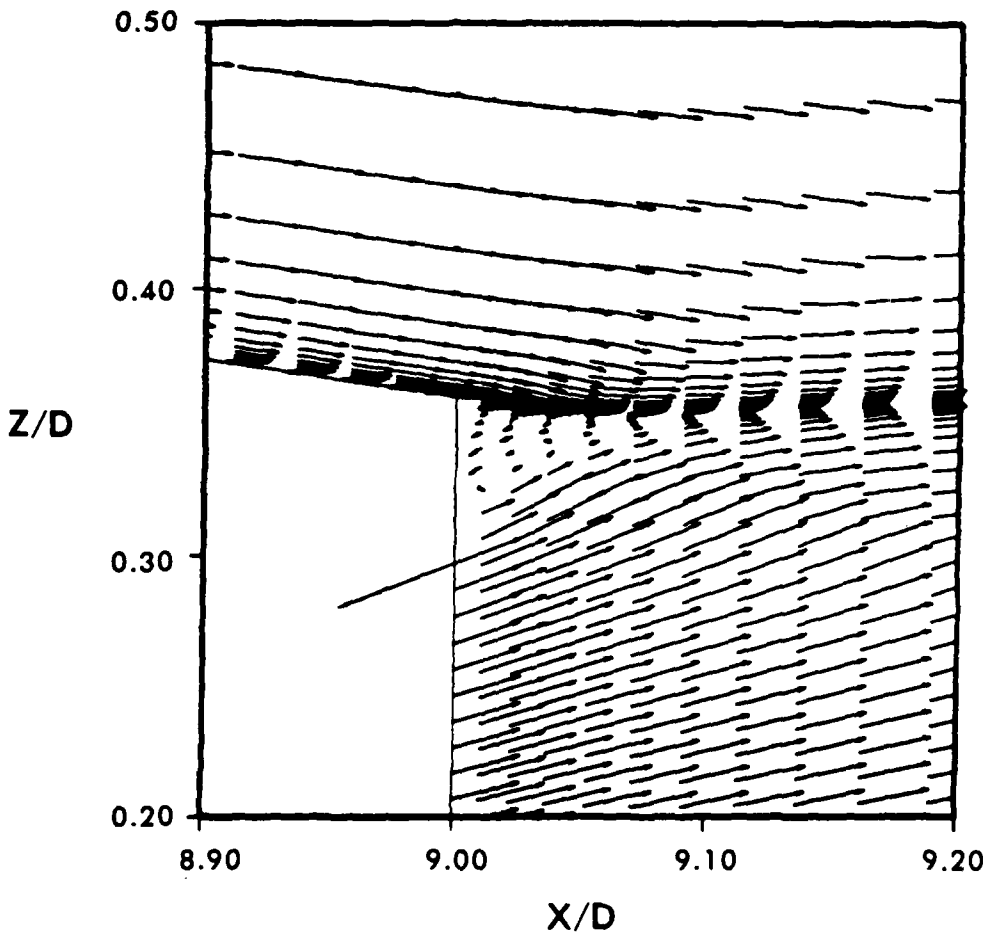

Figure 8b. Velocity vectors expanded near the base corner, M_∞ = 2.0, M_j = 2.5, P_j/P_∞ = 1.0, jet-on.

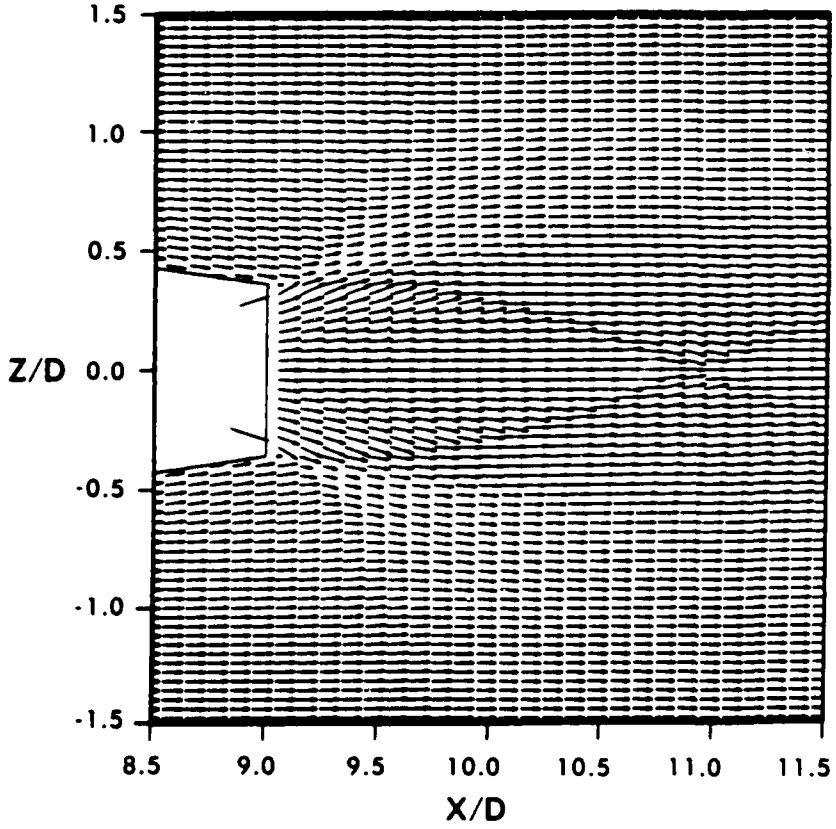

Figure 9. Velocity vectors in the base region, $M_\infty = 2.0$, $M_j = 2.5$, $P_j/P_\infty = 3.0$, jet-on.

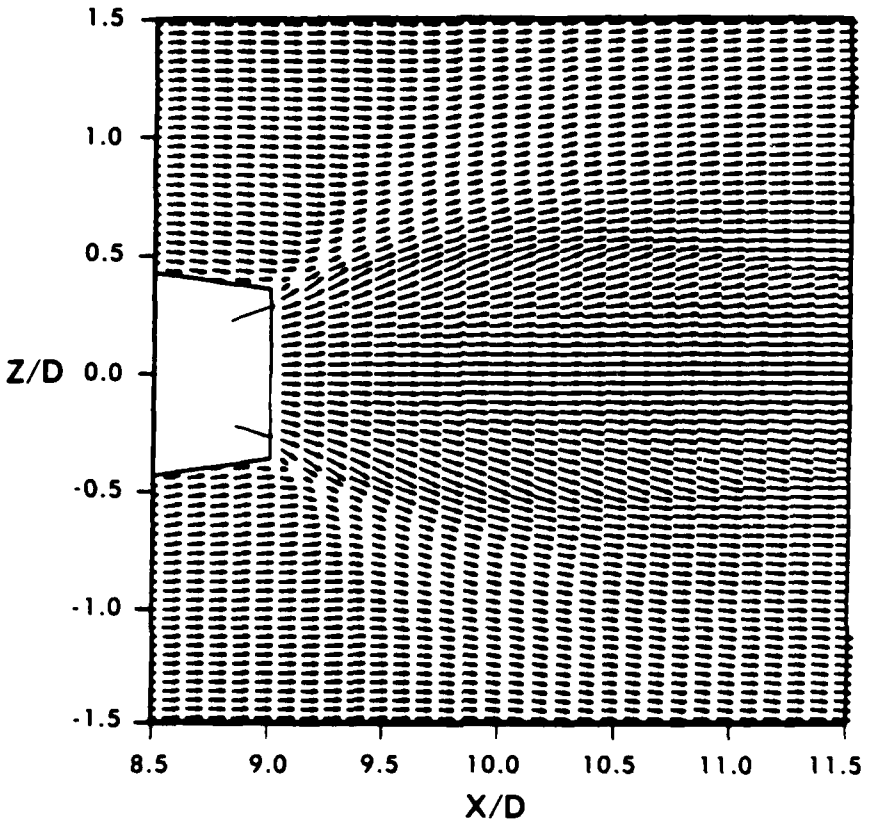

Figure 10a. Velocity vectors in the base region, M_∞ 2.0, M_j = 2.5, P_j/P_∞ = 9.0, jet-on.

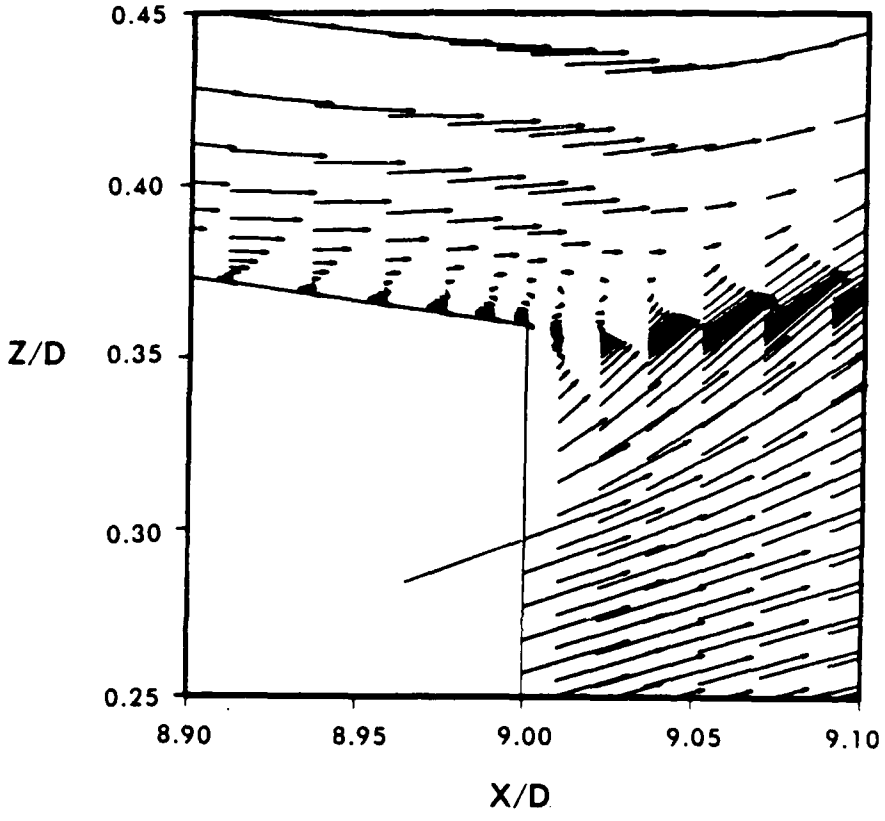

Figure 10b. Velocity vectors expanded near the base corner, $M_\infty = 2.0$, $M_j = 2.5$, $P_j/P_\infty = 9.0$, jet-on.

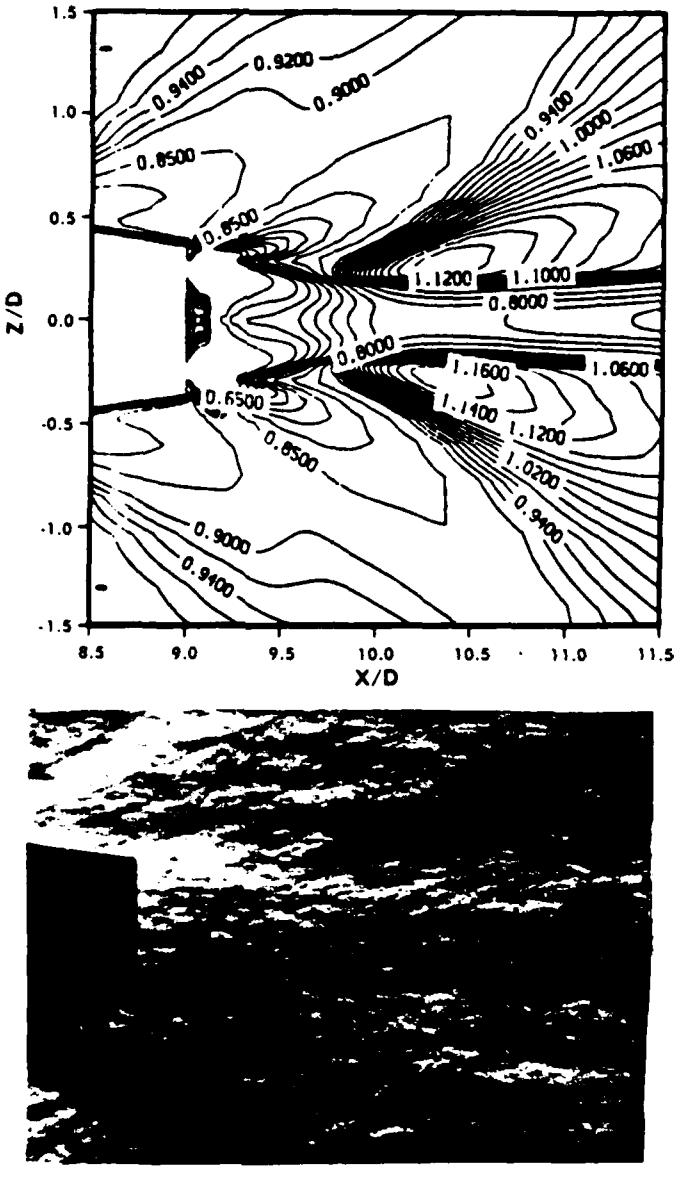

Figure 11. Computed density contours; experimental Schlieren photograph, M_∞ = 2.0, jet-off.

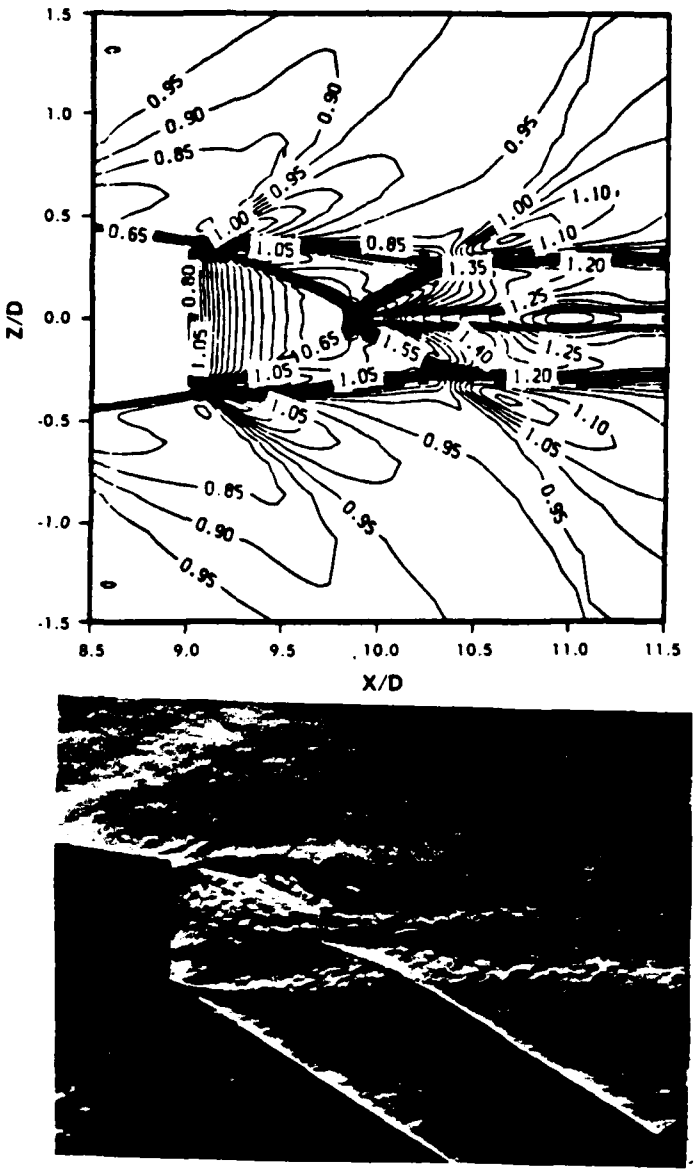

Figure 12. Computed density contours; experimental Schlieren photograph, $M_\infty = 2.0$, $M_j = 2.5$, $P_j/P_\infty = 1.0$, jet-on.

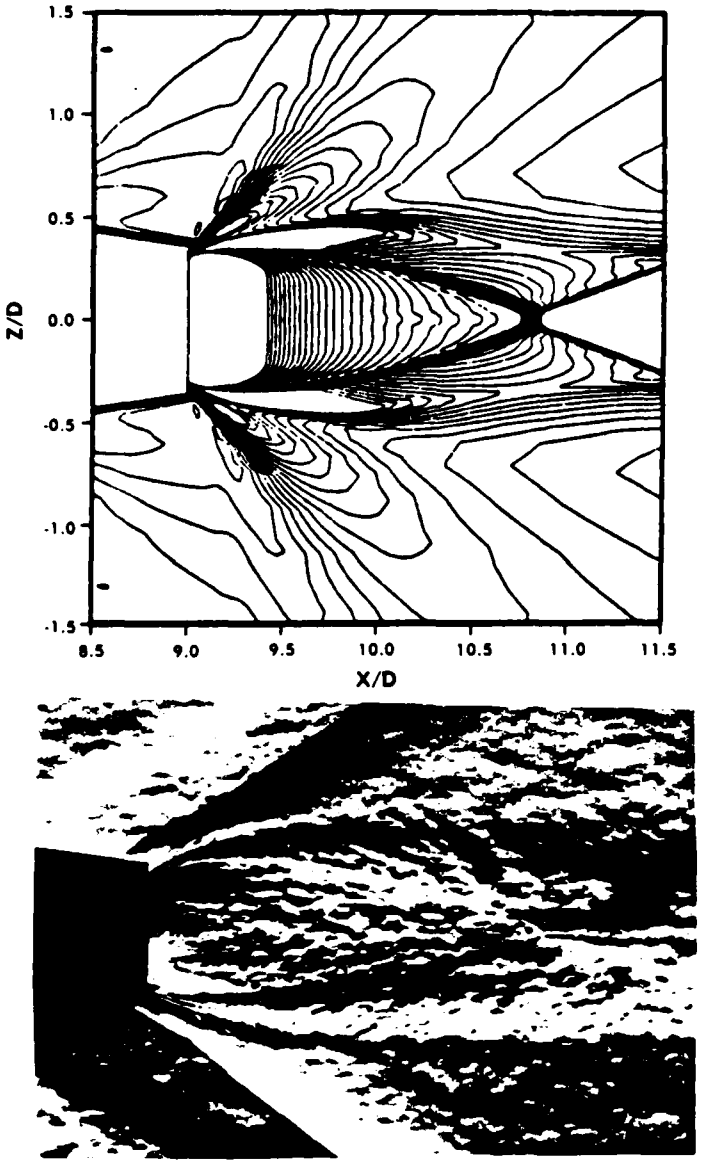

Figure 13. Computational contours; experimental Schlieren photograph, $M_\infty = 2.0$, $M_j = 2.5$, $P_j/P_\infty = 3.0$, jet-on.

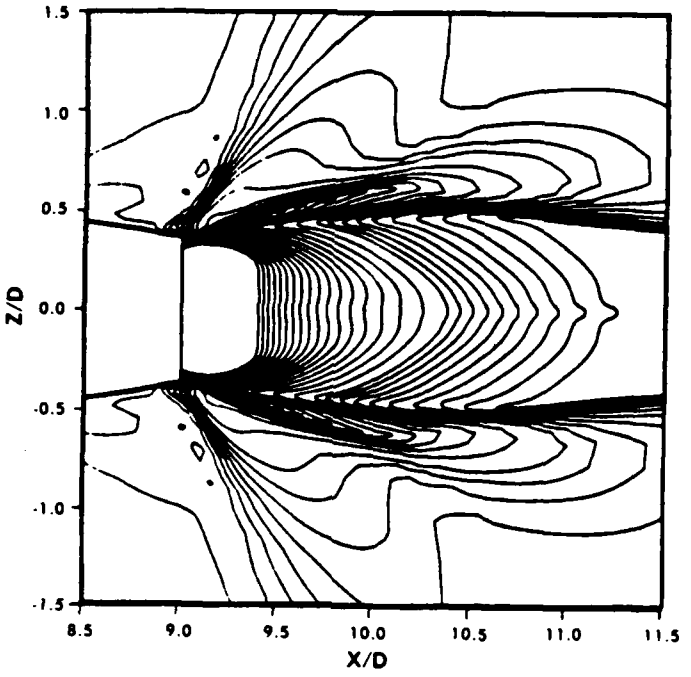

Figure 14. Computed density contours; experimental Schlieren photograph, $M_\infty = 2.0$, $M_j = 2.5$, $P_j/P_\infty = 9.0$, jet-on.

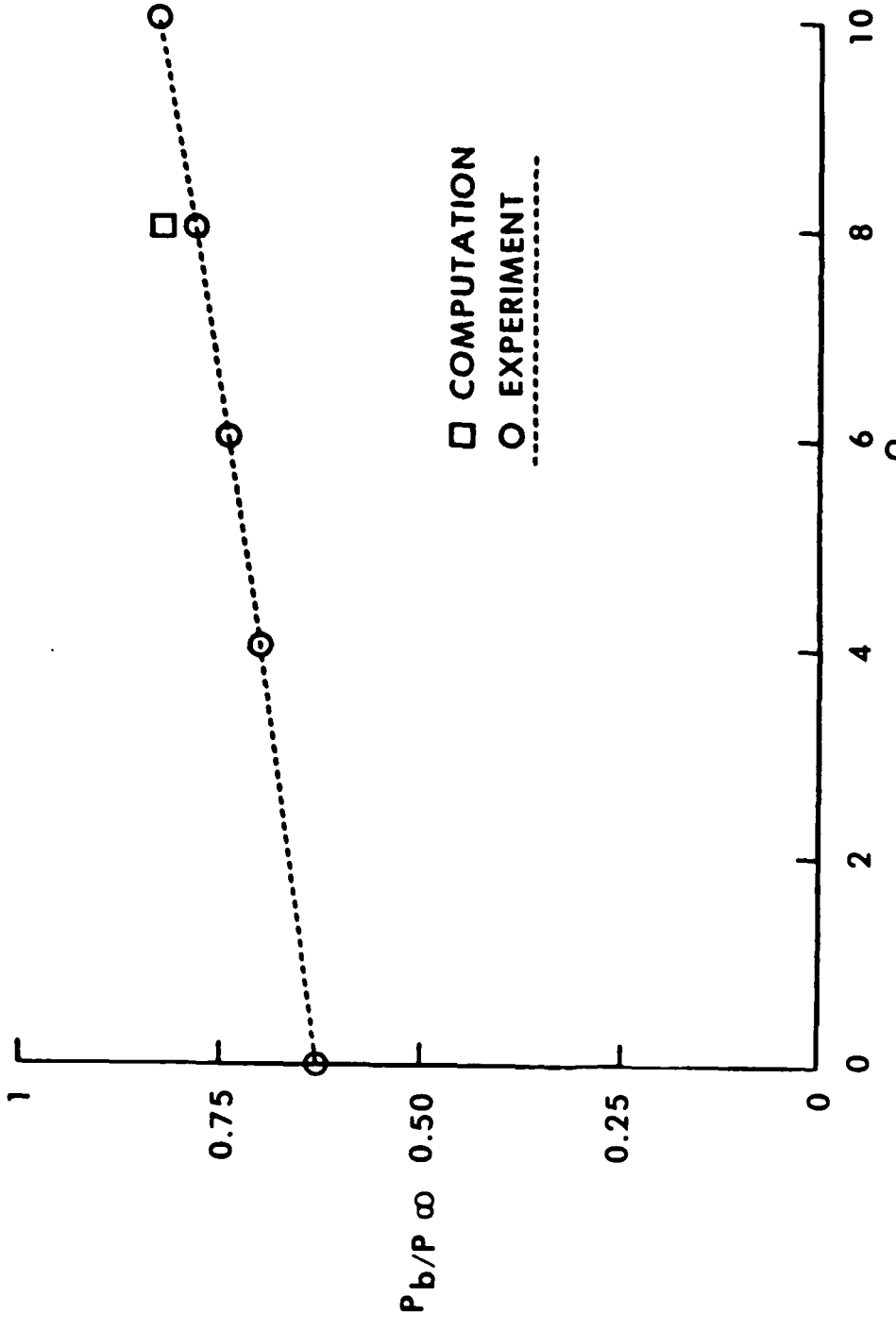

Figure 15. Variation of base pressure with boattail angle, $M_\infty = 2.0$, jet-off.

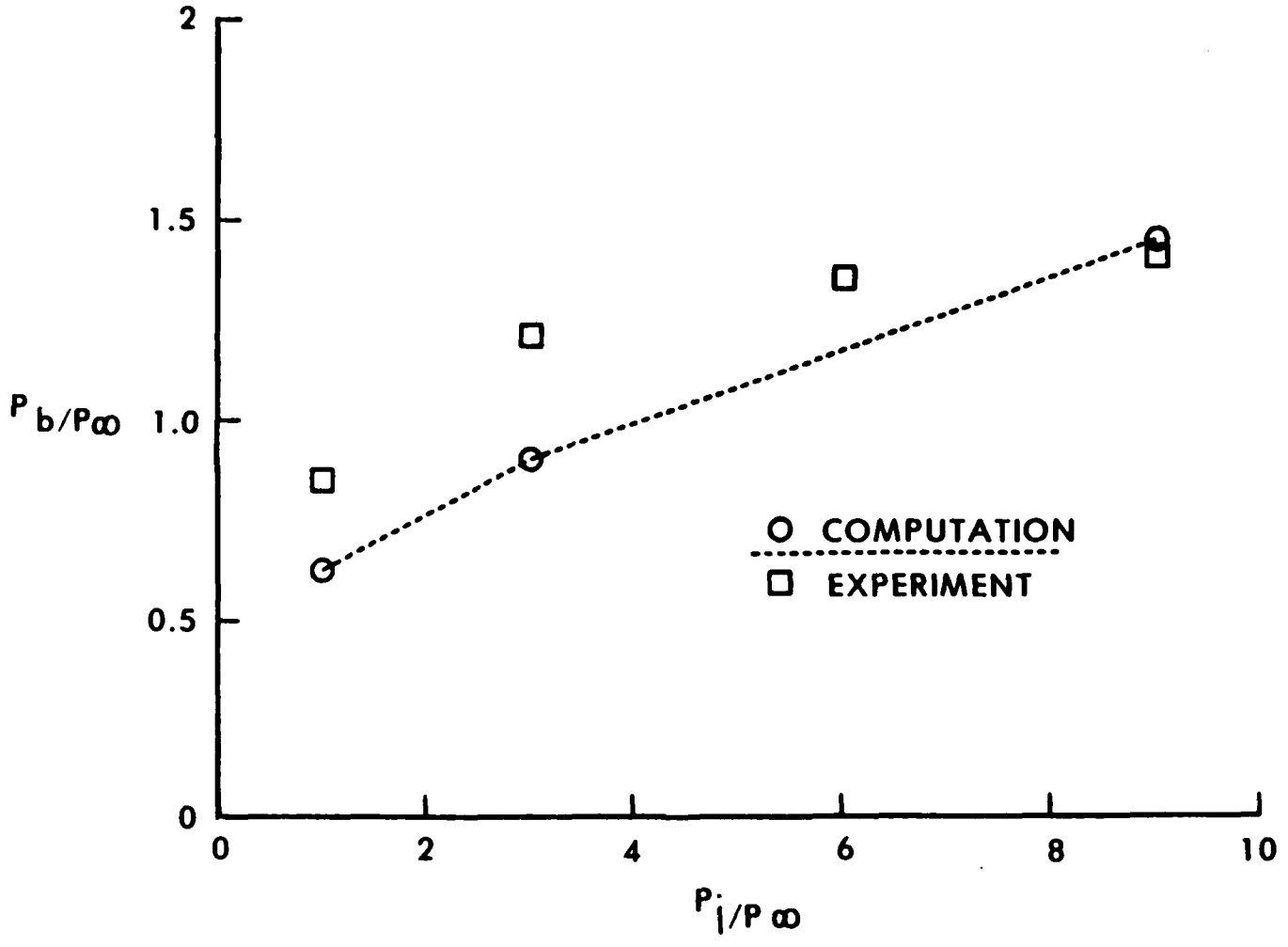

Figure 16. Variation of base pressure with jet pressure, M_∞ = 2.0, jet-on.

REFERENCES

1. Korst, H.H., "A Theory for Base Pressures in Transonic and Supersonic Flow," Journal of Applied Mechanics, December 1956, pp. 593-600.

2. Chow, W.L., "The Effect of Boattailing of a Projectile in Transonic Flow," Proceedings of the Third Symposium on Numerical and Physical Aspects of Aerodynamic Flows, Long Beach, California, June 1985.

3. Sahu, J., Nietubicz, C.J., and Steger, J.L., "Numerical Computation of Base Flow for a Projectile at Transonic Speeds," U.S. Army Ballistic Research Laboratory, Aberdeen Proving Ground, Maryland, ARBRL-TR-02495, June 1983. (AD A130293) (See also, AIAA Paper No. 82-1358, August 1982.)

4. Sahu, J. and Nietubicz, C.J., "Numerical Computation of Base Flow for a Missile in the Presence of a Centered Jet," ARBRL-MR-3397, U.S. Army Ballistic Research Laboratory, Aberdeen Proving Ground, MD, October 1984. (AD A148784) (See also AIAA Paper No. 84-0527, January 1984)

5. Deiwert, G.S., "Supersonic Axisymmetric Flow Over Boattails Containing a Centered Propulsive Jet," AIAA Journal, Vol. 22, No. 10, 1984.

6. Fox, J.H., "Predicting Plume-Induced Separation on Bluff-Base Bodies," AIAA Paper No. 84-0315, January 1984.

7. Wagner, B., "Calculation of Turbulent Flow About Missile Afterbodies Containing an Exhaust Jet," AIAA Paper No. 84-1659, June 1984.

8. Thomas, P.D., et al., "Numerical Simulation of Axisymmetric Base Flow on Tactical Missiles with Propulsive Jet," AIAA Paper No. 84-1658, June 1984.

9. Baldwin, B.S., and Lomax, H., "Thin-Layer Approximation and Algebraic Model for Separated Turbulent Flows," AIAA Paper No. 78-257, 1978.

10. Nietubicz, C.J., Pulliam, T.H., and Steger, J.L., "Numerical Solution of the Azimuthal-Invariant Thin-Layer Navier-Stokes Equations", U.S. Army Ballistic Research Laboratory, Aberdeen Proving Ground, Maryland, ARBRL-TR-02227, March 1980. (AD A085716)

11. Steger, J.L., "Implicit Finite Difference Simulation of Flow About Arbitrary Geometries with Application to Airfoils", AIAA Journal, Vol. 16, No. 4, July 1978, pp. 679-686.

12. Pulliam, T.H. and Steger, J.L., "On Implicit Finite-Difference Simulations of Three-Dimensional Flow", AIAA Journal, Vol. 18, No. 2, February 1980, pp. 159-167.

REFERENCES

13. Beam, R. and Warming, R.F., "An Implicit Factored Scheme for the Compressible Navier-Stokes Equations," AIAA Paper No. 77-645, June 1977.

14. Agrell, J. and White, R.A., "An Experimental Investigation of Supersonic Axisymmetric Flow Over Boattails Containing a Centered Propulsive Jet," FFA Technical Note AU-913, 1974.

LIST OF SYMBOLS

a	speed of sound
A	cross sectional area at the base
C_{D_b}	base drag coefficient, $2\ D_b/\rho_\infty u_\infty^2 A$
c_p	specific heat at constant pressure
C_p	pressure coefficient, $2(p - p_\infty)/\rho_\infty u_\infty^2$
D	body diameter (50mm)
D_b	base drag
e	total energy per unit volume/$\rho_\infty a_\infty^2$
$\hat{E}, \hat{F}, \hat{q}$	flux vector of transformed Navier-Stokes equations
$\hat{H}$	η-invariant source vector
J	Jacobian of transformation
M	Mach number
p	pressure/$\rho_\infty a_\infty^2$
Pr	Prandtl number, $\mu_\infty c_p/\kappa_\infty$
R	body radius
Re	Reynolds number, $\rho_\infty a_\infty D/\mu_\infty$
$\hat{S}$	viscous flux vector
t	physical time
u,v,w	Cartesian velocity components/a_∞

LIST OF SYMBOLS

U,V,W	contravariant velocity components/a_∞
x,y,z	physical Cartesian coordinates
α	angle of attack
γ	ratio of specific heats
κ	coefficient of thermal conductivity/κ_∞
μ	coefficient of viscosity/μ_∞
ξ,η,ζ	transformed coordinates in axial, circumferential and radial directions
ρ	density/ρ_∞
τ	transformed time
ϕ	circumferential angle

Superscript

$*$	critical value

Subscript

b	base
j	jet conditions
J	longitudinal direction
L	normal direction
o	total conditions
st	stagnation conditions
∞	free stream conditions

DISTRIBUTION LIST

No. of Copies	Organization
12	Administrator Defense Technical Info Center ATTN: DTIC-DDA Cameron Station Alexandria, VA 22304-6145
1	HQDA DAMA-ART-M Washington, DC 20310
1	Commander US Army Materiel Command ATTN: AMCDRA-ST 5001 Eisenhower Avenue Alexandria, VA 22333-0001
6	Commander Armament RD&E Center US Army AMCCOM ATTN: SMCAR-TDC SMCAR-TSS SMCAR-LCA-F Mr. D. Mertz Mr. A. Loeb Mr. H. Hudgins Mr. E. Friedman Dover, NJ 07801-5001
	Commander US Army Armament, Munitions & and Chemical Command ATTN: SMCAR-ESP-L Rock Island, IL 61299
1	Director Benet Weapons Laboratory Armament RD&E Center US Army AMCCOM ATTN: SMCAR-LCB-TL Watervliet, NY 12189
1	Commander US Army Aviation Research and Development Command ATTN: AMSAV-E 4300 Goodfellow Blvd. St. Louis, MO 63120

No. of Copies	Organization
1	Director US Army Air Mobility Research and Development Command Ames Research Center Moffett Field, CA 94035
1	Commander US Army Communications - Electronics Command ATTN: AMSEL-ED Fort Monmouth, NJ 07703
1	Commander ERADCOM Technical Library ATTN: DELSD-L (Reports Section) Fort Monmouth, NJ 07703-5301
3	Commander US Army Missile Command Research, Development & Engineering Center ATTN: AMSMI-RD Dr. B. Walker Mr. R. Deep Redstone Arsenal, AL 35898-5500
1	Director US Army Missile & Space Intelligence Center ATTN: AIAMS-YDL Redstone Arsenal, AL 35898-5500
1	Commander US Army Tank Automotive Command ATTN: AMSTA-TSL Warren, MI 48397-5500
1	Director US Army TRADOC Systems Analysis Activity ATTN: ATAA-SL White Sands Missile Range, NM 88002
1	Commander US Army Research Office P. O. Box 12211 Research Triangle Park, NC 27709

DISTRIBUTION LIST

No. of Copies	Organization
1	Commander US Naval Air Systems Command ATTN: AIR-604 Washington, DC 20360
2	Commander US Naval Surface Weapons Center ATTN: Dr. T. Clare, Code DK20 Dr. F. Moore Dahlgren, VA 22448-5000
1	Commander US Naval Surface Weapons Center ATTN: Dr. U. Jettmar Silver Spring, MD 20902-5000
1	Commander US Naval Weapons Center ATTN: Code 3431, Tech Lib China Lake, CA 93555
1	Commander US Army Development and Employment Agency ATTN: MODE-TED-SAB Fort Lewis, WA 98433
1	Director NASA Langley Research Center ATTN: NS-185, Tech Lib Langley Station Hampton, VA 23365
4	Director NASA Ames Research Center ATTN: MS-202-1, Dr. T. Pulliam Dr. J. Steger MS-227-8, Dr. L. Schiff Moffett Field, CA 94035
2	Commandant US Army Infantry School ATTN: ATSH-CD-CSO-OR Fort Benning, GA 31905
1	AFWL/SUL Kirtland AFB, NM 87117
1	Commandant USAFAS ATTN: ATSF-TSM-CN Ft. Sill, OK 73503-5600
1	Air Force Armament Laboratory ATTN: AFATL/DLODL Eglin AFB, FL 32542-5000
2	Sandia Laboratories ATTN: Dr. W.L. Oberkampf Dr. F. Blottner Division 1636 Sandia National Laboratories Albuquerque, NM 87185
1	AEDC Calspan Field Services ATTN: MS 600 (Dr. John Benek) AAFS, TN 37389
1	Virginia Polytechnic Institute & State University ATTN: Dr. Clark H. Lewis Department of Aerospace & Ocean Engineering Blacksburg, VA 24061
1	University of California, Davis Department of Mechanical Engineering ATTN: Prof. H.A. Dwyer Davis, CA 95616
1	Pennsylvania State University Department of Aerospace Engineering ATTN: Dr. G. S. Dulikravich University Park, PA 16802
1	University of Florida Dept. of Engineering Sciences College of Engineering ATTN: Prof. C. C. Hsu Gainesville, FL 32611

DISTRIBUTION LIST

No. of Copies	Organization
10	Central Intelligence Agency Office of Central Reference Dissemination Branch Room GE-47 HQS Washington, DC 20502
1	University of Illinois at Urbana Champaign Department of Mechanical and Industrial Engineering ATTN: Prof. W. L. Chow Urbana, IL 61801
1	University of Maryland Department of Aerospace Engr. ATTN: Dr. J. D. Anderson, Jr. College Park, MD 20742
1	University of Notre Dame Department of Aeronautical and Mechanical Engineering ATTN: Prof. T. J. Mueller Notre Dame, IN 46556
1	University of Texas Department of Aerospace Engineering and Engineering Mechanics ATTN: Dr. D. S. Dolling Austin, Texas 78712-1055
1	University of Delaware Mechanical and Aerospace Engineering Department ATTN: Dr. J.E. Danberg Newark, DE 19711
	Aberdeen Proving Ground
	Dir, USAMSAA ATTN: AMXSY-D AMXSY-MP, H. Cohen
	Cdr, USATECOM ATTN: AMSTE-TO-F
	Cdr, CRDEC, AMCCOM ATTN: SMCCR-RSP-A SMCCR-MU SMCCR-SPS-IL

USER EVALUATION SHEET/CHANGE OF ADDRESS

This Laboratory undertakes a continuing effort to improve the quality of the reports it publishes. Your comments/answers to the items/questions below will aid us in our efforts.

1. BRL Report Number _____ Date of Report _____

2. Date Report Received _____

3. Does this report satisfy a need? (Comment on purpose, related project, or other area of interest for which the report will be used.) _____

_____

_____

4. How specifically, is the report being used? (Information source, design data, procedure, source of ideas, etc.) _____

_____

_____

5. Has the information in this report led to any quantitative savings as far as man-hours or dollars saved, operating costs avoided or efficiencies achieved, etc? If so, please elaborate. _____

_____

_____

6. General Comments. What do you think should be changed to improve future reports? (Indicate changes to organization, technical content, format, etc.)

_____

_____

_____

CURRENT ADDRESS

_____
Name

_____
Organization

_____
Address

_____
City, State, Zip

7. If indicating a Change of Address or Address Correction, please provide the New or Correct Address in Block 6 above and the Old or Incorrect address below.

OLD ADDRESS

_____
Name

_____
Organization

_____
Address

_____
City, State, Zip

(Remove this sheet along the perforation, fold as indicated, staple or tape closed, and mail.)

FOLD HERE

Director
U.S. Army Ballistic Research Laboratory
ATTN: SLCBR-DD-T
Aberdeen Proving Ground, MD 21005-5066

NO POSTAGE
NECESSARY
IF MAILED
IN THE
UNITED STATES

OFFICIAL BUSINESS
PENALTY FOR PRIVATE USE, $300

BUSINESS REPLY MAIL
FIRST CLASS PERMIT NO 12062 WASHINGTON, DC

POSTAGE WILL BE PAID BY DEPARTMENT OF THE ARMY

Director
U.S. Army Ballistic Research Laboratory
ATTN: SLCBR-DD-T
Aberdeen Proving Ground, MD 21005-9989

FOLD HERE

END

12-86

DTIC